PAPER

The fall of an ellipse in a stratified fluid

IOP Publishing | The Japan Society of Fluid Mechanics Fluid Dynamics Research
Fluid Dyn. Res. **56** (2024) 061402 (22pp) https://doi.org/10.1088/1873-7005/ad9861

The fall of an ellipse in a stratified fluid

Erik C Hurlen[1] **and Stefan G Llewellyn Smith**[2,3,*]

[1] William E. Boeing Department of Aeronautics and Astronautics, University of Washington, 1410 NE Campus Pkwy, Seattle, WA 98195, United States of America
[2] Department of Mechanical and Aerospace Engineering, Jacobs School of Engineering, UCSD, 9500 Gilman Drive, La Jolla, CA 92093-0411, United States of America
[3] Scripps Institution of Oceanography, UCSD, 9500 Gilman Drive, La Jolla, CA 92093-0209, United States of America

E-mail: sgls@ucsd.edu and ehurlen@uw.edu

Received 30 June 2024; revised 7 October 2024
Accepted for publication 27 November 2024
Published 10 December 2024

Communicated by Professor Yasuhide Fukumoto

Abstract

The free fall of an ellipse in an infinite linearly-stratified fluid is investigated using a linear two-dimensional, Boussinesq, diffusionless, inviscid model. The oscillations of the ellipse decay because of radiation damping, but unlike the case of a circular cylinder, the ellipse can also rotate and move horizontally. The resulting equations are solved analytically for some simple cases for which there is little or no rotation. Motions with rotation are studied numerically using a spectral method to solve for the wave field in the fluid.

Keywords: stratified flow, internal waves, fluid-structure interaction

1. Introduction

It is an everyday occurrence that objects do not fall in a purely vertical trajectory. One such example is the secondary horizontal motion that can be seen when a coin is thrown into a fountain. A more complicated secondary motion is observed in a falling piece of paper. Flat plates can flutter (periodically oscillating from side to side) or tumble (drifting horizontally while rotating as they fall). This motion is due to the fact that the centre of mass does not coincide with the centre of the resistive stresses provided by the surrounding fluid, hence creating a torque on the object.

The investigation of free-falling bodies goes back to Newton and Galileo. Maxwell (1853) discussed the falling plate problem, including rotation, in a homogeneous fluid. There have been a number of studies of freely falling objects since then. Willmarth *et al* (1964) and then

* Author to whom any correspondence should be addressed.

Field *et al* (1997) studied discs, while Isaacs and Thodos (1967) investigated cylinders, and Lugt (1980) specialized to elliptic cylinders. Mahadevan *et al* (1999) looked at tumbling cards, while Skews (1990) did similar work examining rectangular plates, as did Belmonte and Moses (1999). Tanabe and Kaneko (1994) proposed an ad hoc model for falling paper. Other numerical work includes Huang (2001), Pesavento and Wang (2004), Andersen *et al* (2005a, 2005b), while Jones and Shelley (2005) presented a vortex sheet model and Michelin and Llewellyn Smith (2009) used an unsteady point vortex approach. Field *et al* (1997) provide a good list of references for various applications.

A lot of work has also been carried out on the forced motion of bodies in stratified fluids, with a view to calculating the wave field produced by the body. Internal waves are radiated when an object oscillates in a stratified fluid at a frequency less than the buoyancy frequency, and more generally when particles are displaced from their equilibrium vertical location, such as in a turbulent wake (e.g. Brucker and Sarkar 2010) or when the tide moves over bathymetry, generating the internal tide (e.g. Garrett and Kunze 2007, Sarkar and Scotti 2017). Hurley (1969) studied a cylinder of slender cross-section and Hurley (1972) a circular cylinder, as did Sutherland *et al* (1999) and Appleby and Crighton (1986), who also later also investigated spheres Appleby and Crighton (1987). Hurley (1997) and also Sutherland and Linden (2002) investigated elliptic cylinders, with Hurley (1997) considering translational oscillations alone and Hurley and Hood (2001) considering rotational oscillations. Martin and Llewellyn Smith (2011) examined discs, as did Davis and Llewellyn Smith (2010) who included viscosity theoretically. Much of this work is reviewed in Voisin (2019, 2024a) and Voisin (2024b).

There have also been studies of the drag forces associated with these wave fields. Warren (1960) investigated both cylinders and spheres, as did Ermanyuk (2000), Ermanyuk and Gavrilov (2002) and Ermanyuk and Gavrilov (2003). Torres *et al* (2000) focused on spheres in a numerical study. Higginson *et al* (2003) were concerned with a grid of bars, while Scase and Dalziel (2004) investigated a travelling sphere.

The combination of the above two problems, namely the motion of a freely falling object in a stratified fluid has received less attention. When stratification is introduced, the motion of the solid is also coupled to the wave field, providing an extra physical mechanism affecting the motion. Larsen (1969) looked at the motion of a neutrally buoyant sphere (and a cylinder) in a linearly-stratified inviscid fluid, while Winant (1974) added an empirical nonlinear drag term (see also Cairns *et al* 1979, Andersson and Rahm 1984), and noted that, for small initial displacement of the body compared to its dimension, the amplitude decay of the oscillations is due primarily to radiation damping, while for larger initial displacement the decay is due primarily to viscous attenuation. More recent experiments on oscillating spheres are presented in Chashechkin and Levitskiy (2003), Chashechkin and Prikhod'ko (2006), Prikhod'ko and Chashechkin (2006), Vasil'ev *et al* (2007), Biró *et al* (2008) and Vasil'ev and Chashechkin (2009), while Pyl'nev and Razumeenko (1991) carried out experiments on a thin two-dimensional body elongated along the vertical. Experiments on heavy spheres falling in a stratified fluid are presented in Nikiforovich and Dudchak (1992), Abaid *et al* (2004) and Huguet *et al* (2020).

We draw on Larsen's (1969)'s work, but while in that case the rotation and horizontal motions of the body are zero due to the symmetry of the problem, here we break this symmetry, and therefore the secondary motions of the solid body in the two-dimensional plane are now relevant. Almost all fluids found in the environment are stratified, and most natural bodies are not symmetric. so they will tend to rotate in a non-trivial manner as they fall. As applications, we can mention weather balloons, oceanographic drifters, falling leaves, and so on. Lam *et al* (2018) present experimental results on the fall of heavy discs in a stratified fluid along with a quasi-steady theoretical model that neglects the wave field. Akulenko and Baydulov

(2019) and Baidulov (2022) studied the oscillations of an elliptical float. A general review of the motion of bodies moving in stratified fluids is presented in More and Ardekani (2023).

In this paper we study the motion of an elliptic cylinder in a stably stratified fluid. More specifically, we examine the initial-value problem, that is releasing the solid object from rest after displacing it from its neutrally buoyant position. We carry out a two-dimensional, incompressible, inviscid analysis in an infinite domain. It is expected that the ellipse will oscillate about its stable vertical position with a decaying amplitude due to radiation damping, that is to say the emission of internal waves. Horizontal motions are also expected due to the asymmetry of the body.

In section 2 we formulate the initial-value problem. The ellipse obeys Newton's laws of motion. The fluid properties are calculated using the linearized Boussinesq approximation, under which density variations are taken into account only in calculating buoyancy forces. A constant background stratification of the fluid is assumed, and the governing equations for a two-dimensional incompressible fluid are established. It was noted previously in e.g. Larsen (1969) that the decaying amplitude of oscillation of the solid body is due primarily to radiation damping as opposed to viscous attenuation, and therefore an inviscid model is a natural first step. Due to the complexity of the resulting governing equations for the motion of the ellipse, we implement in section 3 a numerical scheme to solve the problem using spectral method. We conclude in section 4.

2. Mathematical formulation

2.1. Governing equations and coordinate transformations

We will use a frame co-moving with the ellipse and a coordinate system fixed rigidly in the ellipse. This frame is non-inertial and the basic equations for stratified flow, whether written in the co-moving coordinate system or the laboratory coordinate coordinate system, will reflect this, so that pseudoforces will be present. An overview of the link between the coordinates $\mathbf{x}$ in the laboratory frame and $\mathbf{x}_0$ in the co-moving frame is given in the appendix.

To derive the governing equations, we start with the nonlinear Boussinesq equations in two dimensions, written in inertial space:

$$\frac{\mathrm{D}\mathbf{u}}{\mathrm{D}t} = -\nabla p + \sigma \mathbf{j}, \tag{1}$$

$$\nabla \cdot \mathbf{u} = 0, \tag{2}$$

$$\frac{\mathrm{D}\sigma}{\mathrm{D}t} + N^2 v = 0. \tag{3}$$

The Eulerian velocity is $\mathbf{u} = (u, v)^T$, the pressure p is normalized by a mean or representative density value ρ_0, and $\mathbf{j}$ is a unit vector pointing up in the inertial frame. The density has been decomposed as

$$\rho = \rho_0 \left(1 - g^{-1} \int_0^{y'} N^2(\Upsilon)\, \mathrm{d}\Upsilon - g^{-1}\sigma \right), \tag{4}$$

so that σ is the buoyancy. (The lower limit of the integral is arbitrary and corresponds to fixing $\rho_0 = \rho_b(0)$.) Here N is the buoyancy frequency, given by

$$N^2 = -\frac{g}{\rho_0} \frac{\mathrm{d}\rho}{\mathrm{d}y'}. \tag{5}$$

This corresponds to a decomposition of the total pressure, p^T, in the following form: $p^T = p^B(y) + p$, where

$$\frac{\mathrm{d}p^B}{\mathrm{d}y} = -g + \int_0^y N^2(\eta)\,\mathrm{d}\eta s = -g + q(y). \tag{6}$$

The function $q(y)$ depends on the background stratification. For constant N^2, it is given by $q(y) = N^2 y$.

To transfer these equations into non-inertial space, we use the transformation laws derived above in the appendix to obtain

$$\frac{\mathrm{D}\mathbf{u}_0}{\mathrm{D}t} + 2\boldsymbol{\Omega}\times(\mathbf{u}_0+\mathbf{U}_0) + \dot{\boldsymbol{\Omega}}\times(\mathbf{x}_0+\mathbf{X}_0) + \boldsymbol{\Omega}\times[\boldsymbol{\Omega}\times(\mathbf{x}_0+\mathbf{X}_0)] + \dot{\mathbf{U}}_0 = -\nabla_0 p + \sigma\begin{pmatrix}\sin\theta\\ \cos\theta\end{pmatrix}, \tag{7}$$

$$\nabla_0\cdot\mathbf{u}_0 = 0, \tag{8}$$

$$\frac{\mathrm{D}\sigma}{\mathrm{D}t} + N^2\{\sin\theta[u_0 - \Omega(y_0+Y_0) + U_0] + \cos\theta[v_0 + \Omega(x_0+X_0)+V_0]\} = 0, \tag{9}$$

where ∇_0 is the gradient operator in non-inertial space.

We now linearize, which corresponds to replacing convective derivatives by partial time derivatives in the laboratory frame (denoted here by dots). We linearize in the laboratory frame, assuming that $\mathbf{u}$ is the small quantity. Taking just the partial (not total) time derivative of (A.2) when using the transformation laws gives the linearized set of equations

$$\dot{\mathbf{u}}_0 + \boldsymbol{\Omega}\times(\mathbf{u}_0+2\mathbf{U}_0) + \dot{\boldsymbol{\Omega}}\times(\mathbf{x}_0+\mathbf{X}_0) + \boldsymbol{\Omega}\times[\boldsymbol{\Omega}\times(\mathbf{x}_0+\mathbf{X}_0)] + \dot{\mathbf{U}}_0 = -\nabla_0 p + \sigma\begin{pmatrix}\sin\theta\\ \cos\theta\end{pmatrix}, \tag{10}$$

$$\nabla_0\cdot\mathbf{u}_0 = 0, \tag{11}$$

$$\dot{\sigma} + N^2\{\sin\theta[u_0 - \Omega(y_0+Y_0) + U_0] + \cos\theta[v_0 + \Omega(x_0+X_0)+V_0]\} = 0 \tag{12}$$

in the co-moving frame.

From the incompressibility condition, we can define a streamfunction, ψ, by

$$-\frac{\partial\psi}{\partial y_0} = u_0 - \Omega(y_0+Y_0) + U_0, \qquad \frac{\partial\psi}{\partial x_0} = v_0 + \Omega(x_0+X_0) + V_0. \tag{13}$$

This corresponds physically to the streamfunction in inertial space (hence the absence of a 0 subscript). We note that the absolute vorticity in non-inertial space is

$$\zeta_0 + 2\Omega = \partial_{x_0} v_0 - \partial_{y_0} u_0 + 2\Omega = \nabla_0^2\psi. \tag{14}$$

The momentum equations become, in components,

$$\dot{u}_0 - \Omega(v_0+2V_0) - \dot{\Omega}(y_0+Y_0) - \Omega^2(x_0+X_0) + \dot{U}_0 = -p_{x_0} + \sigma\sin\theta, \tag{15}$$

$$\dot{v}_0 + \Omega(u_0+2U_0) + \dot{\Omega}(x_0+X_0) - \Omega^2(y_0+Y_0) + \dot{V}_0 = -p_{y_0} + \sigma\cos\theta. \tag{16}$$

Rewritten entirely in terms of the streamfunction, these take the form

$$-\dot{\psi}_{y_0} - \Omega\psi_{x_0} = -p_{x_0} + \sigma\sin\theta, \tag{17}$$

$$\dot{\psi}_{x_0} - \Omega\psi_{y_0} = -p_{y_0} + \sigma\cos\theta. \tag{18}$$

We hence obtain the vorticity equation

$$\dot{\zeta}_0 + 2\dot{\Omega} = \nabla_0^2\dot{\psi} = \sigma_{x_0}\cos\theta - \sigma_{y_0}\sin\theta = \sigma_x, \tag{19}$$

where the operator acting on σ is just the x-derivative in the non-rotating frame:

$$\partial_x = (\cos\theta)\,\partial_{x_0} - (\sin\theta)\,\partial_{y_0}. \tag{20}$$

The buoyancy equation gives

$$\dot{\sigma} = -N^2\left[\psi_{x_0}\cos\theta - \psi_{y_0}\sin\theta\right] = -N^2\psi_x. \tag{21}$$

Note that N^2 is a known function of y. Finally the pressure equation becomes

$$\nabla_0^2 p = \Omega\nabla_0^2\psi + \sigma_y, \tag{22}$$

where

$$\partial_y = (\sin\theta)\,\partial_{x_0} + (\cos\theta)\,\partial_{y_0}. \tag{23}$$

We are therefore left to solve the set of equations

$$\nabla_0^2\dot{\psi} = \sigma_x, \tag{24}$$

$$\dot{\sigma} = -N^2\psi_x, \tag{25}$$

$$\nabla_0^2 p = \Omega\nabla_0^2\psi + \sigma_y. \tag{26}$$

Now that we have the prognostic equations, we need boundary conditions. On the surface of the object, the normal velocity in the co-moving frame must vanish, i.e. $\mathbf{u}_0\cdot\mathbf{n}_0 = 0$. (We define $\mathbf{n}_0$ to point out from the object into the fluid.) Now the normal is parallel to $(\mathrm{d}y_0, -\mathrm{d}x_0)^T$, so the boundary condition becomes

$$\left\{-\frac{\partial\psi}{\partial y_0} + \Omega\,(y_0 + Y_0) - U_0\right\}\mathrm{d}y_0 + \left\{\frac{\partial\psi}{\partial x_0} - \Omega\,(x_0 + X_0) - V_0\right\}(-\mathrm{d}x_0) = 0. \tag{27}$$

Integrating gives

$$\psi = V_0 x_0 - U_0 y_0 + \frac{1}{2}\Omega\left[(x_0 + X_0)^2 + (y_0 + Y_0)^2\right] - \bar{\psi} \tag{28}$$

on the boundary. This is the boundary condition one would obtain in inertial space by equating the streamfunction to the streamfunction for the rigid-body velocity of the boundary. The term $\bar{\psi}$ is the average of the other terms on the boundary and is there to make sure that Poisson's equation for ψ is well-posed mathematically.

The boundary condition for pressure on the object comes from the momentum equations and takes the form

$$\mathbf{n}_0\cdot\nabla_0 p = \mathbf{n}_0\cdot\begin{pmatrix} \dot{\psi}_{y_0} + \Omega\psi_{x_0} + \sigma\sin\theta \\ -\dot{\psi}_{x_0} + \Omega\psi_{y_0} + \sigma\cos\theta \end{pmatrix}. \tag{29}$$

This can be simplified using the fact that $\mathbf{n}_0\cdot\nabla_0 = \partial_n$ and $\mathbf{n}_0\cdot(\partial_{y_0}\ ,\ -\partial_{x_0})^T = \partial_s$, where n and s are coordinates normal to and along the boundary, respectively. The pressure boundary condition then becomes

$$\partial_n p = \partial_s\dot{\psi} + \Omega\partial_n\psi + \sigma\mathbf{n}_0\cdot\begin{pmatrix} \sin\theta \\ \cos\theta \end{pmatrix}. \tag{30}$$

2.2. Equations of motion for the body

The position of the object is found by solving its equations of motion. The external forces acting on the object are gravity and pressure, which can be decomposed into hydrostatic ($\mathbf{F}^B$) and dynamic ($\mathbf{F}^D$) contributions. (Because pressure has been scaled by ρ_0, these forces are actually per unit mass of the body in the following analysis. The forces in inertial and non-inertial space are related through the rotation matrix R.). Of these, the dynamic pressure is the only one which needs to be calculated using the spectral method presented below. The drawback of this approach is that pseudo-forces appear in the equations of motion in non-inertial space.

The general form of the equations of motion for the ellipse in non-inertial space is

$$\dot{\mathbf{U}}_0 = \mathbf{g}_0 + \mathbf{F}_0^B + \mathbf{F}_0^D + \mathbf{F}_0^C, \tag{31}$$

$$I\dot{\Omega} = G_0^B + G_0^D, \tag{32}$$

where $\mathbf{U}_0 = \dot{\mathbf{X}}_0$, $\Omega = \dot{\theta}$, and I is the moment of inertia of the ellipse divided by its mass. Here $\mathbf{F}_0^C$ represents the pseudo-forces due to the fact we are in a non-inertial reference frame, and is given by

$$\mathbf{F}_0^C = -2\boldsymbol{\Omega} \times \mathbf{U}_0 - \dot{\boldsymbol{\Omega}} \times \mathbf{X}_0 - \boldsymbol{\Omega} \times (\boldsymbol{\Omega} \times \mathbf{X}_0). \tag{33}$$

The forces acting on the object that we can calculate *a priori* are its weight, and the buoyancy force from the hydrostatic pressure, p^B. However, both of these are simpler in the laboratory frame, so we first calculate the nondimensional weight $\mathbf{g} = -g\mathbf{j}$), and then $\mathbf{g}_0 = \mathsf{R}^T\mathbf{g}$. Similarly, $\mathbf{F}_0^B = \mathsf{R}^T\mathbf{F}^B$, where

$$\mathbf{F}^B = -\frac{1}{A}\int_\ell p^B \mathbf{n}\,\mathrm{d}\ell = -\mathbf{j}\frac{1}{A}\int_A \frac{\mathrm{d}p^B}{\mathrm{d}y}\,\mathrm{d}A = \mathbf{j}\left[g - \frac{1}{A}\int_A q(y)\,\mathrm{d}A\right], \tag{34}$$

and A is the area of solid object. As noted previously the equilibrium level of the object is at $y = 0$. Then the first term in $\mathbf{F}^B$ exactly cancels the weight of the object. If N^2 is constant, we can compute the second term in $\mathbf{F}^B$ exactly:

$$-\mathbf{j}\frac{1}{A}\int_A N^2\left[x_0\sin\theta + y_0\cos\theta + Y\right]\mathrm{d}A = -N^2 Y\mathbf{j}. \tag{35}$$

This is just the usual expression for the restoring force of a small particle in a stratified fluid. If N^2 is not constant, $\mathbf{F}^B$ is still vertical but has a more complicated form.

The torque due to the background pressure gradient acting on the object is the same in both inertial and non-inertial space (this is not necessarily true for three dimensions), and can be written as

$$\begin{aligned} G_0^B &= -\frac{1}{A}\int_\ell p\,\epsilon_{3jk}(x_j - X_j)\,n_k\,\mathrm{d}\ell = -\frac{1}{A}\int_A (x - X)\left[-g + q(y)\right]\mathrm{d}A \\ &= -\frac{1}{A}\int_A (x_0\cos\theta - y_0\sin\theta)\,q(x_0\sin\theta + y_0\cos\theta + Y)\,\mathrm{d}A. \end{aligned} \tag{36}$$

If N^2 is constant, the integral can be computed for an ellipse, and becomes

$$G_0^B = -\frac{1}{8}N^2\left(a^2 - b^2\right)\sin 2\theta. \tag{37}$$

It can be shown that $G_0^D = 0$ if $\Omega = \dot{\theta} = 0$. We can then see from equation (32) that $\theta = k\pi/2$ are fixed points of the rotational motion, for any integer k (assuming the ellipse is released

from rotational rest, or $\dot{\theta}_i = 0$, where the subscript i denotes the initial condition). Even values of k correspond to stable fixed points, whereas odd values are unstable.

The dynamic force and torque are given by

$$\mathbf{F}_0^D = -\frac{1}{A}\int p\mathbf{n}_0\,\mathrm{d}\ell \quad \text{and} \quad G_0^D\mathbf{k} = -\frac{1}{A}\int p\mathbf{x}_0\times\mathbf{n}_0\,\mathrm{d}\ell. \tag{38}$$

Since the pressure depends on both the streamfunction and buoyancy field, these will be calculated numerically in the co-moving frame using spectral methods. These methods will be much more efficient if we have a convenient way of expressing the boundary of our object. For an ellipse, we use elliptical coordinates, as follows.

2.3. Elliptical coordinates

Up to this point, the results stated apply to any arbitrarily shaped object, except for (37). We now specialize to the case of an ellipse, where we define the new variables μ and ν such that

$$x_0 = \alpha\cosh\mu\cos\nu, \qquad y_0 = \alpha\sinh\mu\sin\nu. \tag{39}$$

The boundary of the ellipse with major and minor axes of length $2a$ and $2b$, respectively, is given by $\mu = \mu_0$ where

$$\tanh\mu_0 = \frac{b}{a}, \qquad \text{and} \qquad \alpha = \left(a^2 - b^2\right)^{1/2}. \tag{40}$$

With these definitions, we have $x_0 = a\cos\nu$ and $y_0 = b\sin\nu$ on the boundary. Derivatives can be computed from

$$\begin{pmatrix} \mu_{x_0} & \mu_{y_0} \\ \nu_{x_0} & \nu_{y_0} \end{pmatrix} = \alpha h^{-2}\begin{pmatrix} \sinh\mu\cos\nu & \cosh\mu\sin\nu \\ -\cosh\mu\sin\nu & \sinh\mu\cos\nu \end{pmatrix}, \tag{41}$$

where the metric factor is $h \equiv \alpha(\sinh^2\mu + \sin^2\nu)^{1/2}$. The Laplacian becomes

$$\nabla_0^2 = \frac{1}{h^2}\left[\partial_{\mu\mu}^2 + \partial_{\nu\nu}^2\right] = \frac{\alpha^{-2}}{\sinh^2\mu + \sin^2\nu}\left[\partial_{\mu\mu}^2 + \partial_{\nu\nu}^2\right]. \tag{42}$$

We also have on the ellipse $\partial_n = h^{-1}\partial_\mu$ and $\partial_s = h^{-1}\partial_\nu$, and

$$\partial_x = \alpha h^{-2}\left(d_1\partial_\mu - d_2\partial_\nu\right) = \frac{1}{\alpha\left(\sinh^2\mu + \sin^2\nu\right)}\left(d_1\partial_\mu - d_2\partial_\nu\right), \tag{43}$$

$$\partial_y = \alpha h^{-2}\left(d_2\partial_\mu + d_1\partial_\nu\right) = \frac{1}{\alpha\left(\sinh^2\mu + \sin^2\nu\right)}\left(d_2\partial_\mu + d_1\partial_\nu\right), \tag{44}$$

where

$$d_1 = \sinh\mu\cos\nu\cos\theta - \cosh\mu\sin\nu\sin\theta, \tag{45}$$

$$d_2 = \cosh\mu\sin\nu\cos\theta + \sinh\mu\cos\nu\sin\theta. \tag{46}$$

The dynamic force on the ellipse in the co-moving frame is given by

$$\mathbf{F}_0^D = -\frac{1}{A}\int_{\ell_0} p\left(\mathrm{d}y_0\,, -\mathrm{d}x_0\right)^T = -\frac{1}{\pi ab}\int_0^{2\pi} p\left(b\cos\nu, a\sin\nu\right)^T\mathrm{d}\nu. \tag{47}$$

The dynamic torque is the same in both frames. Hence

$$G_0^D = \frac{1}{A}\int_{\ell_0} p\left[x_0\,\mathrm{d}x_0 + y_0\,\mathrm{d}y_0\right] = -\frac{a^2 - b^2}{2\pi ab}\int_0^{2\pi} p\sin 2\nu\,\mathrm{d}\nu. \tag{48}$$

The moment of inertia for an ellipse normalized by mass is $I = (a^2 + b^2)/4$.

To find the forces and torque on the boundary we calculate the pressure from an elliptic problem. However, the boundary condition for the pressure equation involves $\dot{U}_0$, $\dot{V}_0$ and $\dot{\Omega}$, which are given by equations of motion that involve the pressure. The problem is not underdetermined, but these three variables need to be solved for as part of the procedure.

To do this we note that these variables appear linearly in the pressure boundary condition, and that pressure obeys a linear equation. The resulting force is also linear in pressure, so we write

$$\mathbf{F}_0^D = \mathsf{F}_0\dot{\mathbf{U}}_0 + \mathbf{F}_0^\Omega\dot{\Omega} + \mathbf{F}_0^R, \qquad G_0^D = \mathbf{G}_0\cdot\dot{\mathbf{U}}_0 + G_0^\Omega\dot{\Omega} + G_0^R. \tag{49}$$

The linear relations are represented by the matrix F_0, the vectors $\mathbf{F}_0^\Omega$, the row vector $\mathbf{G}_0$ and the scalar G_0^Ω (in three dimensions these are all matrices.) The terms $\mathbf{F}_0^R$ and G_0^R correspond to terms that are independent of the accelerations $\dot{\Omega}$ or $\dot{\mathbf{U}}_0$, which will be calculated numerically.

The terms proportional to $\dot{U}_0$, $\dot{V}_0$, and $\dot{\Omega}$ come from the first term in the pressure boundary condition (30), namely the tangential derivative of the time derivative of the streamfunction on the boundary. This time derivative is obtained from (28), yielding

$$\dot{\psi} = \dot{V}_0 x_0 - \dot{U}_0 y_0 + \frac{1}{2}\dot{\Omega}\left[(x_0+X_0)^2 + (y_0+Y_0)^2\right] + \Omega\left[(x_0+X_0)\,U_0 + (y_0+Y_0)\,V_0\right] - \dot{\bar{\psi}}. \tag{50}$$

Hence we decompose the time derivative of streamfunction and pressure according to

$$\dot{\psi^D} = \dot{U}_0\dot{\psi^U} + \dot{V}_0\dot{\psi^V} + \dot{\Omega}\dot{\psi^\Omega} + \dot{\psi^R}, \qquad p^D = \dot{U}_0 p^U + \dot{V}_0 p^V + \dot{\Omega}p^\Omega + p^R. \tag{51}$$

The functions $\dot{\psi^U}$, $\dot{\psi^V}$ and $\dot{\psi^\Omega}$ are harmonic, as are p^U, p^V and p^Ω. Hoever, we do not actually need to solve for the $\dot{\psi}$ terms since all that matters is their values on the boundary. For the boundary conditions we decompose (50) according to

$$\dot{\psi^U} = -y_0, \qquad \dot{\psi^V} = x_0, \qquad \dot{\psi^\Omega} = \frac{1}{2}\left[(x_0+X_0)^2 + (y_0+Y_0)^2\right]. \tag{52}$$

And

$$\partial_n p^U = \partial_s\psi^U, \qquad \partial_n p^V = \partial_s\psi^V, \qquad \partial_n p^\Omega = \partial_s\psi^\Omega. \tag{53}$$

These fields allow us to compute $\mathsf{F}_0\dot{\mathbf{U}}_0 + \mathbf{F}_0^\Omega\dot{\Omega}$ and $\mathbf{G}_0\cdot\dot{\mathbf{U}}_0 + G_0^\Omega\dot{\Omega}$. In section 3.1 we discuss how to obtain $\mathbf{F}_0^R$ and G_0^R.

Explicitly, for the $\dot{U}_0$ problem we have $\dot{\psi}^U = -y_0 = -b\sin\nu$ on the boundary, so that $p_\mu^U = \psi_\nu^U = -b\cos\nu$ there, along with decay at infinity. This gives $p = be^{\mu_0-\mu}\cos\nu$. Finally we compute

$$-\frac{1}{A}\int p^{U_0}\mathbf{n}_0\,\mathrm{d}\ell = -\frac{1}{\pi ab}\int p^{U_0}\,(b\cos\nu, a\sin\nu)^T\,\mathrm{d}\nu = -\frac{b}{a}\mathbf{i}_0. \tag{54}$$

The $\dot{V}_0$ problem gives the force $-(a/b)\mathbf{j}_0$. We also find that $\mathbf{G}_0$ vanishes. Here $\mathbf{i}_0$ and $\mathbf{j}_0$ represent the directions of the semi-major and semi-minor axes (x_0 and y_0), respectively. For the $\dot{\Omega}$ problem we have $\psi^\Omega = \frac{1}{4}(a^2-b^2)\cos 2\nu + X_0 a\cos\nu + Y_0 b\sin\nu$ on the boundary. Solving the two elementary problems gives

$$\mathbf{F}_0^\Omega = \left(\frac{b}{a}Y_0\,, -\frac{a}{b}X_0\right)^T \qquad G_0^\Omega = -\frac{\left(a^2-b^2\right)^2}{8ab}. \tag{55}$$

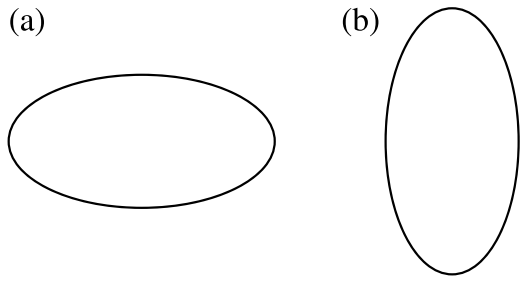

Figure 1. (a) Horizontal (stable) position corresponding to even k. (b) Vertical (unstable) position corresponding to odd k.

We now know all but one of the terms on the right-hand side of the governing equations, which become

$$\left(\frac{1}{4}\left(a^2+b^2\right)+\frac{\left(a^2-b^2\right)^2}{8ab}\right)\dot{\Omega}=-\frac{1}{8}N^2\left(a^2-b^2\right)\sin 2\theta+G_0^R \tag{56}$$

$$\begin{aligned}(1+b/a)\,\dot{U}_0=&-N^2\left(X_0\sin\theta+Y_0\cos\theta\right)\sin\theta+2\Omega V_0\\&+\Omega^2X_0+(1+b/a)\,\dot{\Omega}Y_0+\mathbf{F}_0^R\cdot\mathbf{i}_0\end{aligned} \tag{57}$$

$$\begin{aligned}(1+a/b)\,\dot{V}_0=&-N^2\left(X_0\sin\theta+Y_0\cos\theta\right)\cos\theta-2\Omega U_0\\&+\Omega^2Y_0-(1+a/b)\,\dot{\Omega}X_0+\mathbf{F}_0^R\cdot\mathbf{j}_0\end{aligned} \tag{58}$$

where $\mathbf{F}_0^R$ and G_0^R are found through the spectral method detailed in the next section. The boundary conditions for p^R are

$$\partial_n p^R=\Omega\partial_n\psi+\sigma\mathbf{n}_0\cdot\begin{pmatrix}\sin\theta\\ \cos\theta\end{pmatrix}. \tag{59}$$

Once the forces and hence accelerations are computed, we time step the equations $\mathbf{X}_0$, and hence the motion in the laboratory frame from the relation $\mathbf{X}=\mathsf{R}\mathbf{X}_0$ (and similarly for $\mathbf{U}$).

2.4. Simple cases

Before moving on to the numerical implementation, we analyze some simple cases. The first is the case examined by Larsen (1969) where $a=b$, so that the ellipse is a circular cylinder. The vertical displacement in this case is $Y(t)=Y_iJ_0(Nt)$, where Y_i is the initial vertical displacement, and J_0 is the zeroth-order Bessel function. The horizontal and rotational motions in this case disappear because of the symmetry of the problem.

The second case is when the initial inclination of the ellipse is $\theta_i=0$ or $\theta_i=\pi/2$, and there is no initial angular velocity. Details of the analysis required to obtain (60) are given in Hurlen (2006), section II.1.A. These values of θ_i correspond to fixed points of the rotational motion, as described in the previous section (see figure 1). In this case, the horizontal motion is again 0, and the vertical motion is described by

$$Y(t)=Y_iJ_0\left(Nt\right)+2Y_i\sum_{j=1}^{\infty}\left(\frac{\Lambda-1}{\Lambda+1}\right)^jJ_{2j}\left(Nt\right) \tag{60}$$

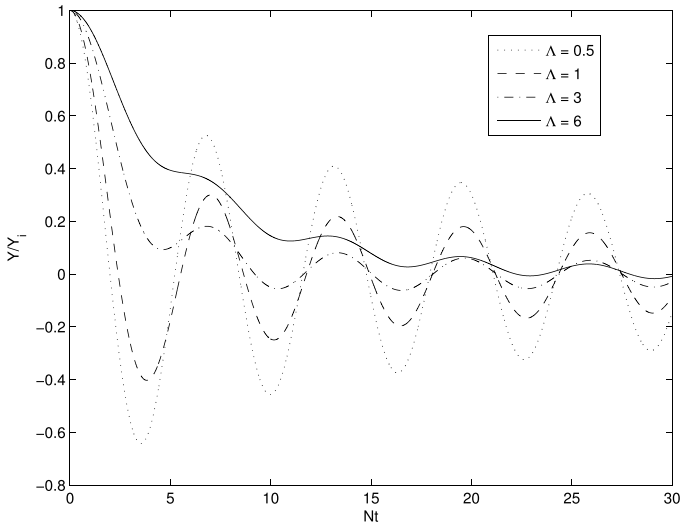

Figure 2. Vertical motion of the horizontal ($\theta = 0$) ellipse for various values of the aspect ratio $\Lambda = a/b$. (The dashed line for $\Lambda = 1$ corresponds to the solution $Y = J_0(Nt)$).

where $\Lambda = a/b$ for even k and $\Lambda = b/a$ for odd k, with $\theta_i = k\pi/2$.

For arbitrary Λ, some interesting behavior can be seen in figure 2. As $\Lambda \to 0$ the solution tends to a sinusoid, and as $\Lambda \to \infty$ the solution tends to $Y = Y_i$, corresponding to the limit of horizontal and vertical flat plates. When $\Lambda = 1$ the solution reduces to the given Bessel function solution for the case $a = b$, as expected. There are other consequences of increasing Λ. For instance, when $\Lambda > 2.5$, the first minimum occurs above the neutrally buoyant position $Y = 0$. When $\Lambda > 5.1$, the first minimum is lost to an inflection point. In this case, it can be seen that the second minimum also occurs above the neutrally buoyant position. Indeed as Λ increases an increasing number of minima occur above $Y = 0$, and an increasing number of minima/maxima are lost to inflection points.

These curves all tend to the solution $Y = (Y_i/\Lambda)J_0(Nt)$ for large times. This behavior is to be expected, since

$$J_K(z) \approx \sqrt{\frac{2}{\pi z}} \cos\left(z - \frac{K\pi}{2} - \frac{\pi}{4}\right) \tag{61}$$

when $z \gg 1$. So, for large Nt, equation (60) becomes

$$Y(t) \approx Y_i \sqrt{\frac{2}{\pi Nt}} \cos\left(Nt - \frac{\pi}{4}\right) \left[1 + 2\sum_{j=1}^{\infty} (-1)^j \left(\frac{\Lambda - 1}{\Lambda + 1}\right)^j\right] = \frac{Y_i}{\Lambda} J_0(Nt). \tag{62}$$

The final case to be analyzed is for the rotational motion, when θ is small. Assuming $\theta \ll 1$, and no initial angular velocity, the solution for this case (to first order in θ) is

$$\theta \approx \theta_i J_0(Nt) + \frac{2\theta_i \left(a^2 - b^2\right)^3}{\pi ab\left(a^2 + b^2\right)^2} \sum_{j=1}^{\infty} B_j J_{2j}(Nt) \tag{63}$$

$$= \theta_i J_0(Nt) + \frac{2\theta_i (-1)^k \left(\Lambda - \Lambda^{-1}\right)^3}{\pi \left(\Lambda + \Lambda^{-1}\right)^2} \sum_{j=1}^{\infty} B_j J_{2j}(Nt), \tag{64}$$

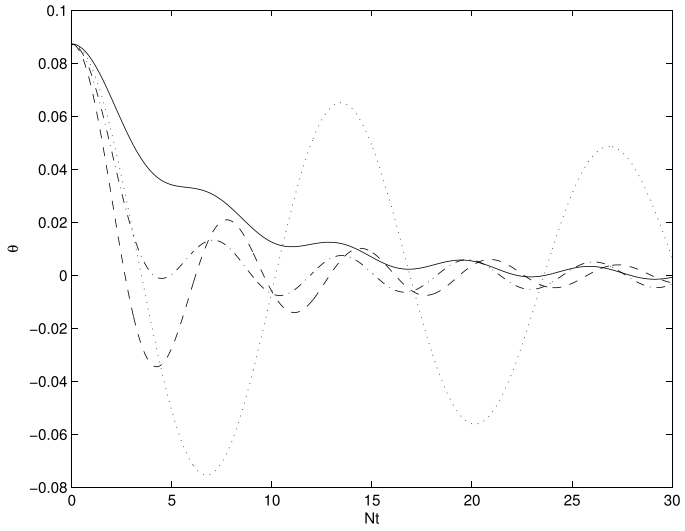

Figure 3. Rotational motion of the ellipse for small initial inclination ($\theta_i \ll 1$), for various values of the aspect ratio $\Lambda = a/b$. Dotted: $\Lambda = 1.25$, dashed: $\Lambda = 2.5$, dash-dot: $\Lambda = 5$, and solid: $\Lambda = 12$. Here $\theta_i = 5^\circ \approx 0.09$ radians.

where

$$B_j = \int_0^{\pi/2} \frac{\cos^2\phi\cos(2j\phi)}{\left(\frac{a^2-b^2}{a^2+b^2} - \sin^2\phi\right)^2 + \frac{(a^2-b^2)^4}{4a^2b^2(a^2+b^2)^2}\sin^2\phi\cos^2\phi}\,\mathrm{d}\phi. \tag{65}$$

We show the results of calculating the B_j numerically in figure 3. The rotational motion for small inclination shares many of the features of the vertical motion. When $\Lambda \gtrsim 5$, the first minimum occurs above $\theta = 0$. We see that this occurs for subsequent minima as Λ is increased, as well as losing minima to inflection points (for $\Lambda > 12$ in this case). However, there are also some new features. For instance, now both the amplitude and frequency of oscillation depend upon Λ. As $\Lambda \to 1$, the frequency goes to zero, along with the decay in amplitude. (This is to be expected, since at $\Lambda = 1$ we would expect no motion whatsoever due to symmetry). As Λ is increased beyond 10, it becomes a bit more difficult to determine general trends due to the increased decay rate.

3. Numerical calculations

3.1. Implementation

We now need to calculate the force, $\mathbf{F}_0^R$. This is basically a modified version of the pressure force, since some of the pressure force has been calculated near the end of section 2.3. We need to solve the fluid equations as given in section 2 to find the pressure on the boundary of the object, removing the previously calculated contributions from $\dot{U}_0$, $\dot{V}_0$, and $\dot{\Omega}$.

We use spectral methods in elliptic coordinates that move with the body. The advantage of this is that the boundary is invariant in time. Further information on spectral methods can be found in Boyd (2000), Trefethen (2000) and Weideman and Reddy (2000). We will use a pseudospectral (or collocation) method. The focus of this paper is not on the numerical scheme used to solve the equations, but rather the solutions themselves, and so we only briefly

describe the procedure used. Most of the method implemented in this work is based on in Trefethen (2000).

We began by setting up differentiation matrices in the μ and ν variables. For the μ direction, since it is a semi-infinite domain and we desire the variables of interest to decay at infinity, we use a Laguerre interpolant. The variable μ begins at $\mu_0 = \tanh^{-1}(b/a)$ as opposed to zero, so we add μ_0 to the polynomial interpolant. For the ν direction, which is periodic, a Fourier matrix is the natural choice.

The scale factors $h = h_\mu = h_\nu$ lead to a diagonal matrix, with the diagonal entries corresponding to the values of h as given in section 2. The other differentiation matrices were then calculated using the basic differentiation matrices. For instance, the Laplacian is calculated using the formula

$$\mathsf{L} = \mathsf{H}^2 \left(\mathsf{D}_\mu^2 + \mathsf{D}_\nu^2 \right) \tag{66}$$

where H is the diagonal matrix mentioned above and D^2 represents the second derivative matrix with respect to the subscripted variable. Similar techniques were used to set up both D_x and D_y (from equation (44)).

The boundary conditions are imposed by replacing the appropriate rows of the differentiation matrix by either the identity (for Dirichlet conditions) or by a row from another differentiation matrix. For example, take the equation for the pressure (59). In elliptic coordinates, this leads to

$$\partial_\mu p^R = \Omega \partial_\mu \psi + \sigma \left(b \cos\nu \sin\theta + a \sin\nu \cos\theta \right). \tag{67}$$

This becomes in matrix notation

$$\mathsf{L} p^R = \Omega \left[\left(-a \sin\nu + X_0 \right) U_0 + \left(b \cos\nu + Y_0 \right) V_0 \right] + \Omega \mathsf{L} \psi + \mathsf{D}_y \sigma = \xi_p. \tag{68}$$

To implement the boundary condition, we replace the boundary rows of the matrix L by the boundary rows in the matrix D_μ, the differentiation matrix representing ∂_μ, and replace the boundary entries of the vector ξ_p by the specified boundary condition. In this case, that is the value of $\Omega \mathsf{D}_\mu \psi + \sigma(b \cos\nu \sin\theta + a \sin\nu \cos\theta)$ on the boundary.

At each time step, the program first calculates p^R. Once this is done, the force and torque components from the pressure are calculated, along with the other moments, G_0^B, G_0^R, and G_0^Ω. From this, the angular acceleration, $\dot{\Omega}$, can be calculated. Then the other forces, $\mathbf{F}_0^\Omega$, $\mathbf{F}_0^R$, F_0, and the pseudo-forces $\mathbf{F}_0^C$ are calculated to find the accelerations in the (x_0, y_0) directions, given by $\ddot{\mathbf{X}}_0$. The program then calculates $\dot{\psi}$ from the Poisson equation (24) and the boundary condition (50), along with $\dot{\sigma}$ from (25) which requires no boundary condition. A time step is then taken to obtain ψ and σ. Once this is done, the motion and velocity of the ellipse in the co-moving frame, $\mathbf{X}_0$ and $\mathbf{U}_0$, are found by time stepping. The motion of the ellipse in the laboratory frame ($\mathbf{X}$) is then calculated at each instant in time using the relation $\mathbf{X} = \mathsf{R}\mathbf{X}_0$ (and similarly for the velocity). The time stepping is carried out using a built-in MATLAB ODE solver, `ode15s`. A solver for stiff problems helps since there is a time scale associated with ν, while the pressure equation is elliptic so that information is propagated immediately

To get an indication of the error involved in this numerical scheme, we examine the case $\theta_i = 0$. We know the exact solution for Y in this particular case, and θ remains 0. Hence we obtain an indication of the error associated with both vertical and rotational motions. We analyzed the results for various values of m and n, the degrees of the polynomial interpolant in the μ and ν variables respectively. It was found that an appropriate value of n needs to be taken to make sure that the solution is qualitatively correct, and then increasing m increased the accuracy.

In the experiments of Larsen (1969), with a large sphere (i.e. large Stokes number) and small initial displacement, the oscillations of the sphere were effectively finished after about ten buoyancy periods. Hence we examine solutions up to $Nt = 30$. For situations with small Stokes number and large initial displacements so that viscosity is important, which is not the relevant parameter regime here, the experiments of Biró *et al* (2008) indicated oscillations over a larger number of periods.

3.2. Vertical motion

For all the numerical results, the program was set to the following conditions. It was found that $m = 16$ and $n = 48$ provided adequate precision over the time range of interest. We also set the buoyancy frequency $N = 1$, with $Y_i = b$, and $X_i = 0$ (to match the majority of experiments). In all the figures the data for θ is given in radians, and the X and Y results are normalized by Y_i (or equivalently b).

We began by analyzing the case of a circular cylinder ($a = b$) to verify the results. The numerics for this case follow what is given above, except we need to use a different coordinate system, since the elliptic system is singular when $a = b$. We use the coordinates

$$x = a\mathrm{e}^{r}\cos\vartheta, \qquad y = a\mathrm{e}^{r}\sin\vartheta. \tag{69}$$

In this system, r acts like μ and ϑ like ν. The derivatives are

$$\partial_x = \frac{\mathrm{e}^{-r}\cos\vartheta}{a}\partial_r - \frac{\mathrm{e}^{-r}\sin\vartheta}{a}\partial_\vartheta, \qquad \partial_y = \frac{\mathrm{e}^{-r}\sin\vartheta}{a}\partial_r + \frac{\mathrm{e}^{-r}\cos\vartheta}{a}\partial_\vartheta. \tag{70}$$

The scale factors are again equal and given by $h = h_r = h_\vartheta = a\mathrm{e}^{r}$, so that the Laplacian is given by

$$\nabla^2 = (a\mathrm{e}^{r})^{-2}\left(\partial_{rr}^2 + \partial_{\vartheta\vartheta}^2\right). \tag{71}$$

The boundary conditions become

$$\dot{\psi} = \dot{V}a\cos\vartheta, \qquad p_r = \dot{\psi}_\vartheta + a^{-1}\sigma\sin\vartheta. \tag{72}$$

We also need to calculate the pressure integrals in equation (38) numerically. This is done by summing the contribution at each boundary point using

$$-\mathbf{i}\cdot\int_C p\,\mathrm{d}\mathbf{S} \approx \sum pa\cos\vartheta\Delta\vartheta, \qquad -\mathbf{j}\cdot\int_C p\,\mathrm{d}\mathbf{S} \approx \sum pa\sin\vartheta\Delta\vartheta. \tag{73}$$

(This is the trapezoidal or midpoint rule, which is exponentially accurate for periodic integrands.) The integrated pressure in the horizontal direction should be zero by symmetry with no horizontal motion. This is a useful test to make sure the program functions correctly.

The solution produced here compares very well with the analytic solution, as shown in figure 4(a). The error between the two solutions had a very similar form and amplitude to that of the following case, shown in figure 4(b), in which there is no rotational motion, and $\theta_i = k\pi/2$. We determined analytical solutions in these cases in the previous section, and comparison between those and the numerical solution shows good agreement, as can be seen in figure 4. The two solutions differ by no more than 4.5×10^{-3} over the entire interval.

3.3. Energy budget

A useful check on the numerical procedure is to examine the energy budget of the system. We outline this budget for the case of a cylinder, in which case rotation does not feature. It is easiest to work in an inertial frame when dealing with the energy (which is frame dependent).

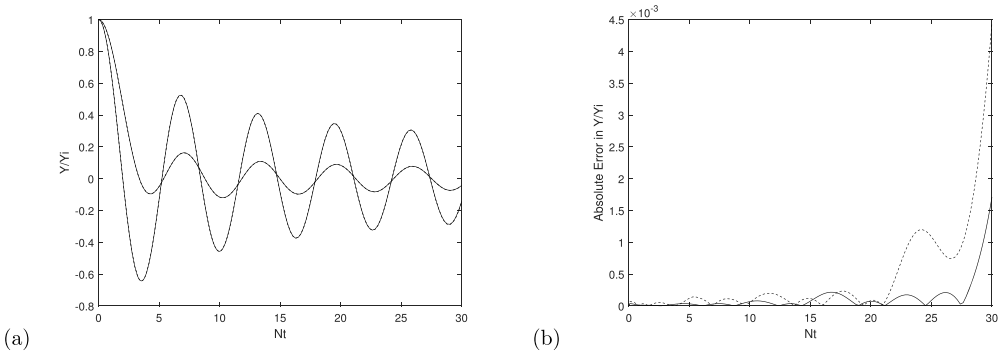

Figure 4. (a) Comparison between the numeric (solid) and analytic (dashed) solutions for $\theta_i = \pi/2$ (large amplitude solution) and $\theta_i = \pi$ (smaller amplitude). The lines are indistinguishable. (b) Absolute error between the theoretical and numerical solutions in each case. Solid: $\theta_i = \pi$, dashed: $\theta_i = \pi/2$.

The total energy of the cylinder is

$$E_s = \frac{\rho_0}{2}\left(\pi a^2 \mathbf{U}^2 + \pi a^2 N^2 Y^2\right), \tag{74}$$

made up of a kinetic and a potential term, while the total energy of the fluid is

$$E_f = \int_A \left(|\mathbf{u}'|^2 + \frac{\sigma^2}{N^2}\right) \mathrm{d}A, \tag{75}$$

where the integral is over the fluid domain. The transfer of energy from solid to fluid can be written as

$$\Delta E_c^f = \pi a^2 \mathbf{U}\cdot\mathbf{F}^D = -\int p_b \mathbf{n}\cdot\mathbf{U} = -\Delta E_f^c = \int_A \mathbf{u}\cdot\nabla p \,\mathrm{d}A, \mathrm{d}\vartheta. \tag{76}$$

The two integrals are equal by the divergence theorem, but can be computed separately for the cylinder and fluid quantities respectively as a check on the numerics. Since the ϑ discretization is equispaced in the spectral code, the first integral reduces to a sum over boundary points. To compute integrals over the fluid region numerically, consider the integral $\int_A \chi^2 \,\mathrm{d}A$, for some general function χ. The first step is to change to the coordinates used in the spectral method, that is to the variables r and ϑ. This is done using the scale factors $h = a\mathrm{e}^r$, so that

$$\int_A \chi^2 \,\mathrm{d}A = \int\int \chi^2 h^2 \,\mathrm{d}r\mathrm{d}\vartheta = \int_0^{2\pi}\int_0^{r_{\max}} a^2\chi^2\mathrm{e}^{2r}\mathrm{d}r\mathrm{d}\vartheta. \tag{77}$$

The discretization in ϑ is trivial since it simply becomes a sum over each point,

$$\int_0^{2\pi}\int_0^{r_{\max}} a^2\chi^2\mathrm{e}^{2r}\mathrm{d}r\mathrm{d}\vartheta \approx \sum_{k=1}^{n}\int_0^{r_{\max}} a^2\left(\chi\left(r,\vartheta_k\right)\right)^2\mathrm{e}^{2r}\mathrm{d}r\frac{2\pi}{n}. \tag{78}$$

For the radial discretization, we invert the appropriate differentiation matrices.

With the resolution used, the energy starts to diverge around $Nt = 22$ (see figure 5). This can be removed by increasing the resolution. The implication is that computation of the fluid properties is more sensitive to the numerical resolution than the motion of the solid cylinder. Calculating the energy balance of the system hence gives an indication of when it is necessary to increase the resolution.

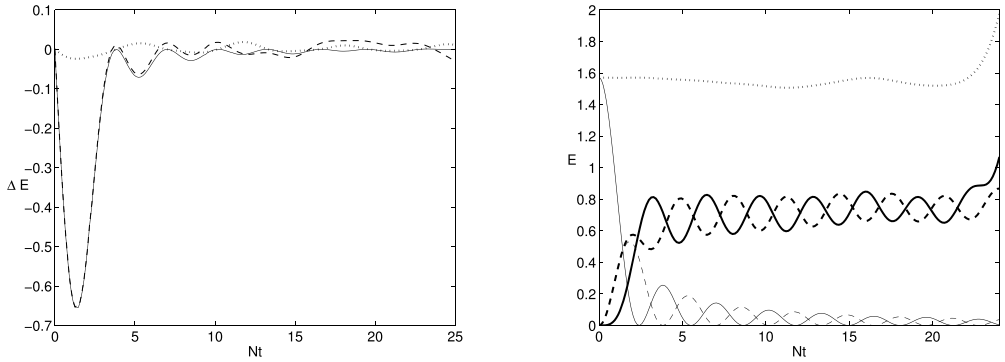

Figure 5. Left: the solid line is the energy transferred from the cylinder $(\Delta E)^s_f$; the dashed line is the negative of the energy transferred from the fluid $(\Delta E)^f_s$, and the dotted line is energy passing through the boundary (from the Reynolds transport terms), and should be equal to the time derivative of the total energy curve shown on the right. Right: total energy. The dotted line is the total energy of the system, dashed lines are kinetic energies, while solid lines are potential energies. The thick lines correspond to the fluid, while the thin lines are for the solid cylinder.

The total energy of the solid decreases in time, while that of the fluid initially increases, then levels off as expected. Finally, the total energy of the system remains relatively constant, but does decrease slightly in time, due to the radiation of energy through the outer boundary.

Extending this analysis to the case of an ellipse is straightforward for the most part. The integrals have different scale factors, and the integrals themselves now go around the boundary of an ellipse. One also needs account for the rotational energy. These extra terms come from the rotational equation, and are given by a kinetic term and a potential term,

$$E^r_k = \frac{1}{2} I\Omega^2 \quad \text{and} \quad E^r_p = \frac{1}{8} N^2 \left(a^2 - b^2\right) \sin^2\theta. \tag{79}$$

In addition there is also an amount of this energy which is transferred to the fluid, computed via the integral

$$(\Delta E)^r = \int \Omega G^D \mathrm{d}A. \tag{80}$$

3.4. Results

After these checks we examine motion with varying θ. We begin with small initial inclinations to compare to the previously determined approximate solution for this case. This approximation is very close up to $\theta_i = 5^\circ$ and fairly close up to $\theta_i = 10^\circ$. The results shown in figure 3, are indistinguishable when $\theta_i = 5^\circ$.

Typical results for intermediate values of θ_i and Λ are shown in figure 6. Both θ and Y are decaying oscillatory functions. Results for larger values of these two variables are shown in figure 7.

We note the following behaviors of the falling ellipse. First, as in figures 2 and 3, the ellipse does not fall (or rotate as the case may be) below the neutrally buoyant position on the first cycle for large enough values of Λ. Further increasing Λ results in this being more prominent. For cases when the ellipse was inclined initially, the motion is more complicated. However, we did

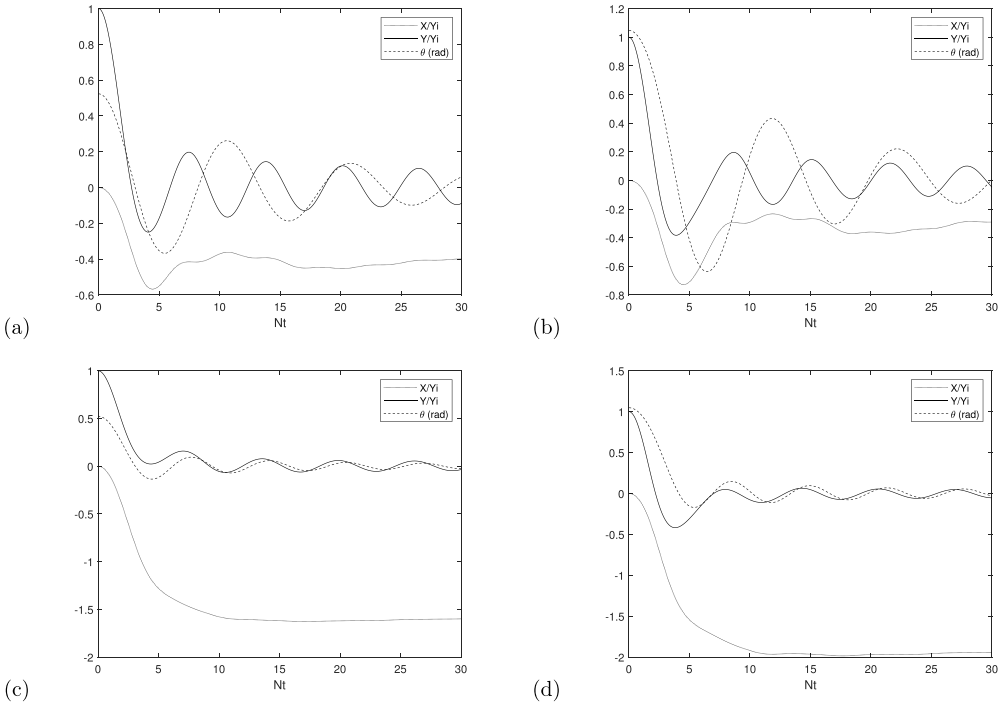

Figure 6. Numerical results for (a) $\Lambda = 1.5$ and $\theta_i = \pi/6$, (b) $\Lambda = 1.5$ and $\theta_i = \pi/3$, (c) $\Lambda = 3$ and $\theta_i = \pi/6$, (d) $\Lambda = 3$ and $\theta_i = \pi/3$. Dashed line is θ, solid line is Y, and dotted line is X.

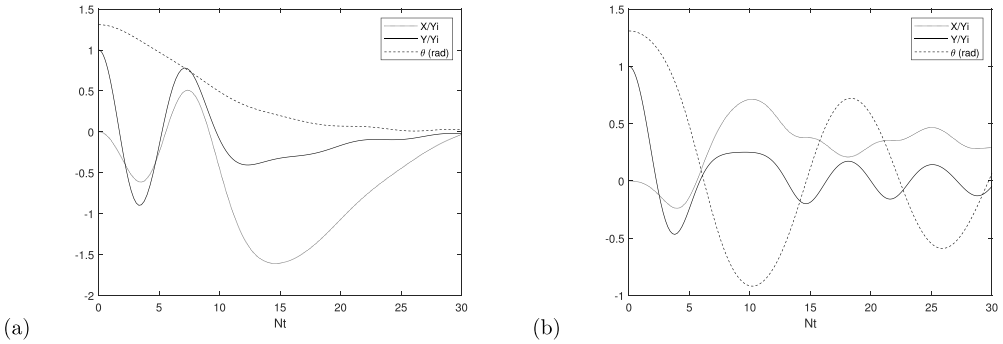

Figure 7. Numerical results for $\theta_i = 75^\circ$. (a) $\Lambda = 10$, (b) $\Lambda = 1.25$. Dashed line is θ, solid line is Y, and dotted line is X.

not observe a tumbling regime. Presumably such motions depends on nonlinear interactions, which are not present in the current formulation.

We examine the parameter space in figure 8. It can be seen in figure 8(a) that there is almost a linear relation between Λ and the time at which the ellipse first drops below its neutrally buoyant position. This is most obvious at larger values of Λ. At smaller values, there are discrete jumps, which amount to a local minimum being above the plane $Y = 0$. This occurs for the larger values as well, but in these cases only one data point lies within each division, since

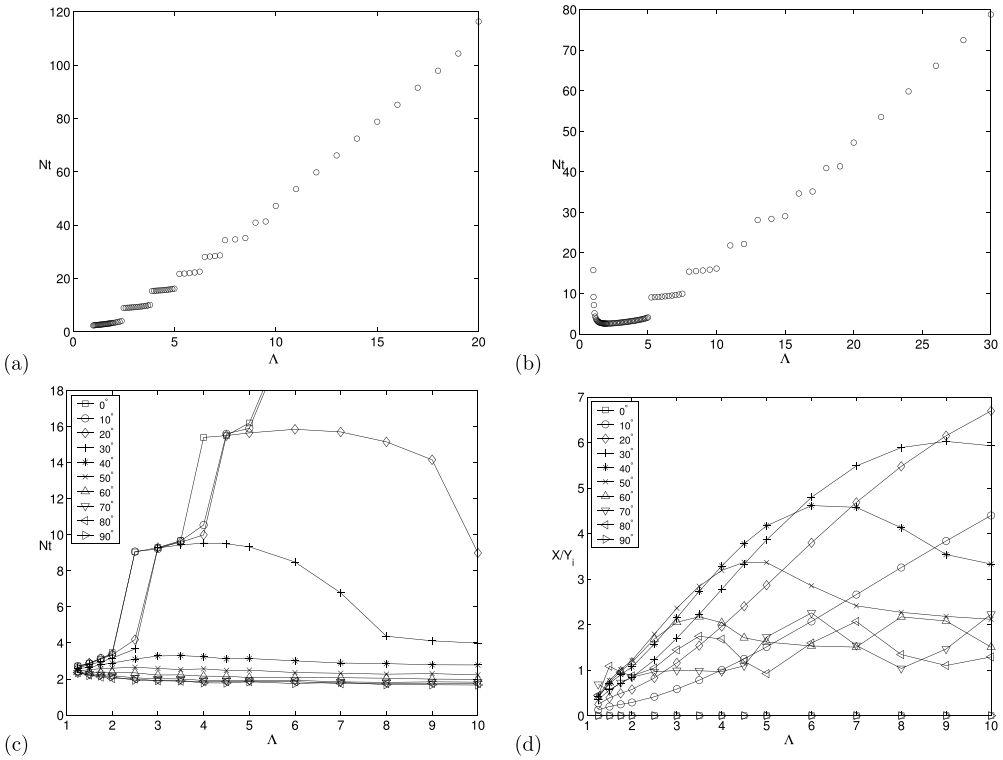

Figure 8. Examination of the parameter space of the numerical results. (a) Time at which the solution of the vertical motion first becomes negative with $\theta_i = 0$, as a function of Λ. This corresponds to the first instant at which the ellipse drops below its neutrally buoyant position, as in figure 2. (b) Time at which the solution of the rotational motion first becomes negative as a function of Λ, for small initial inclination as in figure 3. (c) Time at which the vertical motion first becomes negative as a function of Λ for various values of θ_i. (d) Maximum deviation of the horizontal motion of the ellipse, that is, the maximum value of X as a function of Λ for various values of θ_i.

the values of Λ which were analyzed were clustered near the smaller values. These jumps occur at roughly $\Lambda \approx 2.5, 3.9, 5.1, 6.4, \ldots$, as can be seen in figure 2. Similar behaviour is seen in (2.17) and figures 2(a), (c), (e), (g) and (i) of Voisin (2024a). In figure 8(b), we can see similar behaviour for the rotational motion, although there are some differences. For instance, there are fewer jumps over the same interval of Λ, with them now occurring at $\Lambda \approx 5.1, 7.7, 10.3, \ldots$. Another difference is in the behaviour at smaller values of Λ. Whereas the time remained relatively constant over the intervals for the vertical motion, it can be seen that this is not the case for the rotational motion, most noticeably in the first interval when $\Lambda \leqslant 5$. This, however, is expected as it is clear from figure 3 that the frequency of oscillation is dependent upon Λ, which was not the case in figure 2.

The real challenge of this analysis comes when the initial inclination angle is not restricted to be small. This is the case in parts (c) and (d) of figure 8. The first of these shows the first time at which the ellipse falls below the neutrally buoyant position as a function of both Λ and θ_i. It can be seen that increasing θ_i beyond 50° basically assures that the ellipse will fall below its neutrally buoyant position in its first cycle. The type of motions encountered in these cases is similar to that shown in figure 7(a). It is also interesting to note that these times decrease

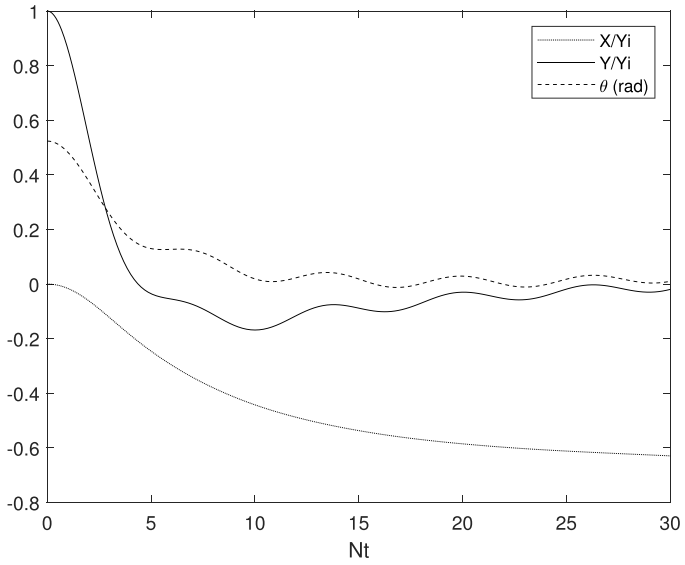

Figure 9. Numerical results for $\Lambda = 8$ and $\theta_i = 30^\circ$. Dashed line is θ, solid line is Y, and dotted line is $X/10$ (renormalized for clarity).

as Λ is increased for certain values of θ_i, most notably 20° and 30°. To get a better idea as to what exactly is happening in these cases, the results for $\Lambda = 8$ and $\theta_i = 30$ degrees are plotted in figure 9 (where the magnitude of the horizontal motion has been decreased by a factor of 10 to better show the other motions).

It seems reasonable to expect the maximum horizontal deviations to come at intermediate values of θ_i, and large values of Λ. Figure 8(d) reinforces this notion, although there are some interesting behaviors present. First of all, we can see that there is no horizontal motion for the cases $\theta_i = 0$ or 90 degrees, as expected. Also, for smaller values of Λ, higher values of θ_i (70 and 80 degrees) produce larger values of $X_{\max}$. As Λ is increased (between 2 and 6), we see the intermediate value of θ_i (40 and 50 degrees) produce the largest deviations, as postulated. However, as Λ is increased further, $\theta_i = 30$ and then 20 degrees begin to produce the largest horizontal motion. The larger values of θ_i begin to drop off as Λ is increased, and that they even begin to oscillate.

4. Conclusion

The motion of an ellipse in a stratified fluid was determined analytically for a variety of orientations. In addition numerical results were obtained using a spectral method in the cases where it was not possible to determine analytic solutions. It was found that this method produced accurate results when compared to analytic solutions.

Hurlen (2006) presented laboratory experiments that were carried out to compare to the analytic results. These consist of vertically displacing an elliptic cylinder from its neutrally buoyant position in salt stratified water, holding it fixed with its major axis inclined at an angle with respect to the horizontal while the fluid comes to rest, and then releasing it so that it can oscillate and rotate freely as it falls. The subsequent motion was recorded, from which data about the motion was extracted.

These experiments yielded encouraging results as the general trends agreed, but the motion in the experiments was damped in comparison to the theory. The experimental results oscillate and decay quicker than their numerical counterparts. The discrepancy is presumably in our linear and inviscid assumptions, as well as in the finite size of the tank, but was not quantified. New experiments with more sophisticated equipment would help in understanding the motion and comparing it to the present results.

Unlike the case of translating objects, here the body has no imposed velocity, and will emit waves as it starts to fall, suggesting that the influence of wave drag should dominate over form drag. In the present formulation, the linear (added mass) component of form draft is present, but nonlinear effects are not included. Comparisons to experiments or simulations would be needed to assess their size.

One way to quantify the inaccuracies would be to add viscosity and non-linearity to the present analysis. With the current setup this is possible conceptually, but difficult in practice. Viscosity and density diffusion lead to extra terms on the right-hand side of the field equations, giving

$$\nabla_0^2\dot{\psi} = \sigma_x + \gamma\nabla^4\psi, \tag{81}$$

$$\dot{\sigma} = -N^2\psi_x + \kappa\nabla^2\sigma, \tag{82}$$

$$\nabla_0^2 p = \Omega\nabla_0^2\psi + \sigma_y, \tag{83}$$

where γ and κ represent the viscosity and diffusivity respectively. The first difficulty is that the no-slip boundary condition increases the order of the differential equations, and the exact results for buoyancy in § 2 come from simple solutions of the Laplace's equation, which is no longer appropriate. Voisin (2024a) developed a model in which the viscous damping of the oscillations is caused by viscous dissipation in the oscillatory boundary layer, which compared favorably with experiments in the literature. Defining a Stokes number $St = Na^2/\nu$, the model is valid for $St < 100$ say, with viscosity negligible for $St > 1000$ say.

Adding in non-linear terms makes the problem much more difficult. Such an effort enters the realm of DNS, as in Torres *et al* (2000), but also including coupling beween fluid and solid, for example using an Immersed Boundary Method approach, e.g. as applied by More *et al* (2021) to the free fall of a spheroid.

Our results provide a start to understanding the motion of asymmetric objects falling in stratified fluids. Possible applications include processes ranging from ocean sediments and seed dispersal to vehicle dynamics. With such considerations in mind, we leave more accurate experiments and DNS for future work

Acknowledgments

This work was funded by NSF Grant CTS-0133978. We are grateful to Glenn Ierley, Bruno Voisin and Michael Le Bars for helpful discussions.

Appendix. Relation between laboratory and co-moving coordinates

Denote the coordinates in the laboratory frame by $\mathbf{x} = (x, y)^T$ and in the co-moving frame by $\mathbf{x}_0 = (x_0, y_0)^T$. The two are related by

$$\mathbf{x} = \mathsf{R}(t)\,\mathbf{x}_0 + \mathbf{X}(t) = \mathsf{R}(t)\,[\mathbf{x}_0 + \mathbf{X}_0(t)]\,, \tag{A.1}$$

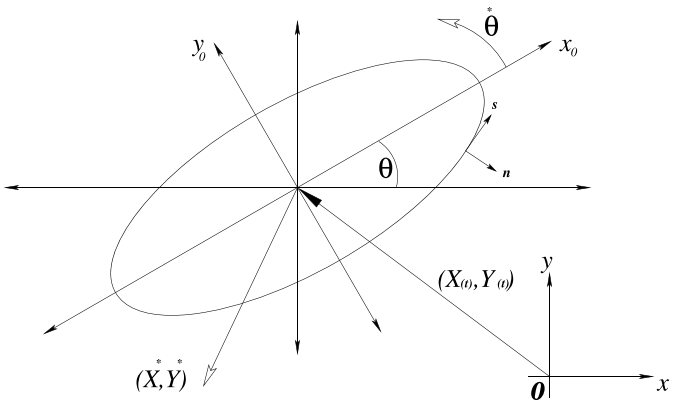

Figure A1. Relationship between θ and axes (x, y) (laboratory frame) and (x_0, y_0) (co-moving frame).

where $\mathsf{R}(t)$ is an orthogonal rotation matrix such that $\mathsf{R}^T\mathsf{R} = \mathsf{R}\mathsf{R}^T = \mathsf{I}$, where I is the identity matrix. The vector $\mathbf{X}(t)$ is the position vector of the centre of the co-moving frame in the laboratory frame, while $\mathbf{X}_0(t)$ is the same vector in the co-moving frame. The two are related by $\mathbf{X}(t) = \mathsf{R}(t)\mathbf{X}_0(t)$. The transformation law (A.1) is appropriate for the motion of a rigid body.

Now differentiate (A.1) with respect to time, considering all terms as functions of time. This corresponds to calculating the Lagrangian velocity and subsequently acceleration of a particle. Now there is a distinction between velocity with respect to inertial space in the laboratory frame, $\mathbf{u} = \mathrm{D}\mathbf{x}/\mathrm{D}t$, and velocity with respect to non-inertial space in the co-moving frame, $\mathbf{u}_0 = \mathrm{D}\mathbf{x}_0/\mathrm{D}t$. We have

$$\mathbf{u} = \mathsf{R}\left[\mathbf{u}_0 + \mathbf{U}_0 + \mathsf{O}\left(\mathbf{x}_0 + \mathbf{X}_0\right)\right], \tag{A.2}$$

where $\mathsf{O} \equiv \mathsf{R}^T\dot{\mathsf{R}}$ is the angular velocity matrix, and $\dot{\mathsf{R}} = \mathsf{R}\mathsf{R}^T\dot{\mathsf{R}} = \mathsf{R}\mathsf{O}$ and $\dot{\mathbf{X}}_0 = \mathbf{U}_0$. Since R is orthogonal, we have $\mathsf{R}^T\dot{\mathsf{R}} + \dot{\mathsf{R}}^T\mathsf{R} = 0$, which shows that O is antisymmetric and hence acts as a cross product: $\mathsf{O}\mathbf{a} = \boldsymbol{\Omega} \times \mathbf{a}$, where $\boldsymbol{\Omega}$ is the angular velocity vector (given by $\boldsymbol{\Omega} = \dot{\theta}\mathbf{k}$ in two dimensions), for an arbitrary vector $\mathbf{a}$.

The acceleration comes from

$$\frac{\mathrm{D}\mathbf{u}}{\mathrm{D}t} = \mathsf{R}\left[\frac{\mathrm{D}\mathbf{u}_0}{\mathrm{D}t} + \dot{\mathbf{U}}_0 + 2\mathsf{O}\left(\mathbf{u}_0 + \mathbf{U}_0\right) + \dot{\mathsf{O}}\left(\mathbf{x}_0 + \mathbf{X}_0\right) + \mathsf{O}^2\left(\mathbf{x}_0 + \mathbf{X}_0\right)\right]. \tag{A.3}$$

Here we can identify the standard translational, Coriolis, transverse, and centripetal terms associated with accelerated coordinate systems. In two dimensions we have

$$\mathsf{R} = \begin{pmatrix} \cos\theta & -\sin\theta \\ \sin\theta & \cos\theta \end{pmatrix}, \qquad \mathsf{O} = \dot{\theta}\begin{pmatrix} 0 & -1 \\ 1 & 0 \end{pmatrix}, \qquad \mathsf{O}^2 = -\dot{\theta}^2\mathsf{I}, \tag{A.4}$$

where θ is the angle that the co-moving frame makes with the inertial frame (see figure A1). For further reference we have the operator ∇_0 given by $\nabla_0 = (\partial_{x_0}, \partial_{y_0})^T = \mathsf{R}^T\nabla = \mathsf{R}^T(\partial_x, \partial_y)^T$.

ORCID iD

Stefan G Llewellyn Smith https://orcid.org/0000-0002-1419-6505

References

Abaid N, Adalsteinsson D, Agyapong A and McLaughlin R 2004 An internal splash: levitation of falling spheres in stratified fluids *Phys. Fluids* **16** 1567–80

Akulenko L D and Baydulov V G 2019 Extreme properties of oscillations of an elliptical float *Dokl. Phys.* **64** 297–300

Andersen A, Pesavento U and Wang Z J 2005a Analysis of transitions between fluttering, tumbling and steady descent of falling cards *J. Fluid Mech.* **541** 91–104

Andersen A, Pesavento U and Wang Z J 2005b Unsteady aerodynamics of fluttering and tumbling plates *J. Fluid Mech.* **541** 65–90

Andersson L and Rahm L 1984 On the dynamics of a neutrally-buoyant float in a non-linear stratified fluid *Geophysica* **19** 157–67

Appleby J C and Crighton D G 1986 Non-Boussinesq effects in the diffraction of internal waves from an oscillating cylinder *Q. J. Mech. Appl. Math.* **39** 209–31

Appleby J C and Crighton D G 1987 Internal gravity waves generated by oscillations of a sphere *J. Fluid Mech.* **183** 439–50

Baidulov V G 2022 Parametric control of float oscillations *Mech. Solids* **57** 562–9

Belmonte A and Moses E 1999 Flutter and tumble in fluids *Phys. World* **12** 21–25

Biró I, Szabó K G, Gyüre B, Jánosi I M and Tél T 2008 Power-law decaying oscillations of neutrally buoyant spheres in continuously stratified fluid *Phys. Fluids* **20** 051705

Boyd J P 2000 *Chebyshev and Fourier Spectral Methods* 2nd edn (Dover)

Brucker K A and Sarkar S 2010 A comparative study of self-propelled and towed wakes in a stratified fluid *J. Fluid Mech.* **652** 373–404

Cairns J, Munk W and Winant C 1979 On the dynamics of neutrally buoyant capsules; an experimental drop in Lake Tahoe *Deep-Sea Res.* **26A** 369–81

Chashechkin Y D and Levitskiy V V 2003 Pattern of flow around a sphere oscillating an neutrally buoyancy horizon in a continuously stratified fluid *J. Vis.* **6** 59–65

Chashechkin Y D and Prikhod'ko Y V 2006 The structure of flows occurring under the free oscillations of a cylinder on the neutral-buoyancy horizon in a continuously stratified fluid *Dokl. Phys.* **51** 215–8

Davis A J M and Llewellyn Smith S G 2010 Tangential oscillations of a circular disk in a viscous stratified fluid *J. Fluid Mech.* **656** 342–59

Ermanyuk E V 2000 The use of impulse response functions for evaluation of added mass and damping coefficient of a circular cylinder oscillating in linearly stratified fluid *Exp. Fluids* **28** 152–9

Ermanyuk E V and Gavrilov N V 2002 Force on a body in a continuously stratified fluid. Part 1. Circular cylinder *J. Fluid Mech.* **451** 421–43

Ermanyuk E V and Gavrilov N V 2003 Force on a body in a continuously stratified fluid. Part 2. Sphere *J. Fluid Mech.* **494** 33–50

Field S B, Klaus M, Moore M G and Nori F 1997 Chaotic dynamics of falling disks *Nature* **388** 252–4

Garrett C and Kunze E 2007 Internal tide generation in the deep ocean *Annu. Rev. Fluid Mech.* **39** 57–87

Higginson R C, Dalziel S B and Linden P F 2003 The drag on a vertically moving grid of bars in a linearly stratified fluid *Exp. Fluids* **34** 678–86

Huang J Y 2001 Moving coordinates methods and applications to the oscillations of a falling slender body *Moving Boundaries VI: Computational Modelling of Free and Moving Boundary Problems* ed B Šarler and C A Brebbia (WIT Press) pp 73–82

Huguet L, Barge-Zwick V and Le Bars M 2020 Dynamics of a reactive spherical particle falling in a linearly stratified fluid *Phys. Rev. Fluids* **5** 114803

Hurlen E C 2006 The motions and wave fields produced by an ellipse moving through a stratified fluid *PhD Thesis* University of California San Diego

Hurley D G 1969 The emission of internal waves by vibrating cylinders *J. Fluid Mech.* **36** 657–72

Hurley D G 1972 A general method for solving steady-state internal gravity wave problems *J. Fluid Mech.* **56** 721–40

Hurley D G 1997 The generation of internal waves by vibrating elliptic cylinders. Part 1: Inviscid solution *J. Fluid Mech.* **351** 105–18

Hurley D G and Hood M J 2001 The generation of internal waves by vibrating elliptic cylinders. Part 3. Angular oscillations and comparison of theory with recent experimental observations *J. Fluid Mech.* **433** 61–75

Isaacs J L and Thodos G 1967 The free-settling of solid cylindrical particles in the turbulent regime *Can. J. Chem. Eng.* **45** 150–5
Jones M A and Shelley M J 2005 Falling cards *J. Fluid Mech.* **540** 393–425
Lam T, Vincent L and Kanso E 2018 Passive flight in density-stratified fluids *J. Fluid Mech.* **860** 200–23
Larsen L H 1969 Oscillations of a neutrally buoyant sphere in a stratified fluid *Deep-Sea Res.* **16** 587–603
Lugt H J 1980 Autorotation of an elliptic cylinder about an axis perpendicular to the flow *J. Fluid Mech.* **99** 817–40
Mahadevan L, Ryu W S and Samuel A 1999 Tumbling cards *Phys. Fluids* **11** 1–3
Martin P A and Llewellyn Smith S G 2011 Generation of internal gravity waves by an oscillating horizontal disc *Proc. R. Soc.* A **467** 3406–23
Maxwell J C 1853 On a particular case of the decent of a heavy body in a resisting medium *Camb. Dublin Math. J.* **9** 145–8
Michelin S and Llewellyn Smith S G 2009 An unsteady point vortex method for coupled fluid–solid problems *Theor. Comp. Fluid Dyn.* **23** 127–53
More R V and Ardekani A M 2023 Motion in stratified fluids *Annu. Rev. Fluid Mech.* **55** 157–92
More R V, Ardekani M N, Brandt L and Ardekani A 2021 Orientation instability of settling spheroids in a linearly density-stratified fluid *J. Fluid Mech.* **929** A7
Nikiforovich Y I and Dudchak K P 1992 Fall of a rigid, thermally-conducting sphere through a thermally stratified fluid *Fluid Mech. Res.* **21** 7–14
Pesavento U and Wang Z J 2004 Falling paper: Navier–Stokes solutions, model of fluid forces and center of mass elevation *Phys. Rev. Lett.* **93** 144501
Prikhod'ko Y V and Chashechkin Y D 2006 Hydrodynamics of natural oscillations of neutrally buoyant bodies in a layer of continuously stratified fluid *Fluid Dyn.* **41** 545–54
Pyl'nev Y V and Razumeenko Y V 1991 Damped oscillations of a float of special shape, deeply immersed in a homogeneous and stratified fluid *Mech. Solids* **26** 67–76
Sarkar S and Scotti A 2017 From topographic internal gravity waves to turbulence *Annu. Rev. Fluid Mech.* **49** 125–220
Scase M M and Dalziel S B 2004 Internal wave fields and drag generated by a translating body in a stratified fluid *J. Fluid Mech.* **498** 289–313
Skews B W 1990 Autorotation of rectangular plates *J. Fluid Mech.* **217** 33–40
Sutherland B R, Dalziel S B, Hughes G O and Linden P F 1999 Visualization and measurement of internal waves by 'Synthetic Schlieren'. Part 1: vertically oscillating cylinder *J. Fluid Mech.* **390** 93–126
Sutherland B R and Linden P F 2002 Internal wave excitation by a vertically oscillating elliptic cylinder *Phys. Fluids* **14** 721–31
Tanabe Y and Kaneko K 1994 Behavior of falling paper *Phys. Rev. Lett.* **73** 1372–5
Torres C R, Hanazaki H, Ochoa J, Castillo J and Woert M V 2000 Flow past a sphere moving vertically in a stratified diffusive fluid *J. Fluid Mech.* **417** 221–36
Trefethen L N 2000 *Spectral Methods in Matlab* (SIAM)
Vasil'ev A Y and Chashechkin Y D 2009 Damping of the free oscillations of a neutral buoyancy sphere in a viscous stratified fluid *J. Appl. Math. Mech.* **73** 558–65
Vasil'ev A Y, Kistovich A V and Chashechkin Y D 2007 Free oscillations of a balanced ball on the horizon of neutral buoyancy in a continuously stratified fluid *Dokl. Phys.* **52** 596–9
Voisin B 2019 Boundary integrals for oscillating bodies in stratified fluids *J. Fluid Mech.* **927** A3
Voisin B 2024a Added mass of oscillating bodies in stratified fluids *J. Fluid Mech.* **987** A27
Voisin B 2024b Buoyancy oscillations *J. Fluid Mech.* **984** A29
Warren F M G 1960 Wave resistance to vertical motion in a stratified fluid *J. Fluid Mech.* **7** 209–29
Weideman J A C and Reddy S 2000 A MATLAB differentiation matrix suite *ACM Trans. Math.* **26** 465–519
Willmarth W W, Hawk N E and Harvey R L 1964 Steady and unsteady motions and wakes of freely falling disks *Phys. Fluids* **7** 197–208
Winant C D 1974 The descent of neutrally buoyant floats *Deep-Sea Res.* **21** 445–53